

Redox Active Mesoporous Hybrid Materials by In situ Syntheses with Urea-linked Triethoxysilylated Phenothiazines

Zhou Zhou,^[a] Adam W. Franz,^[b] Sarah Bay,^[b] Biprajit Sarkar,^[c] Andreas Seifert,^[d] Piaoping Yang,^[e] Alex Wagener,^[a] Stefan Ernst,^[a] Markus Pagels,^[f] Thomas J. J. Müller,^{*,[b]} and Werner R. Thiel^{*,[a]}

Dedicated to Prof. Dr. Stefan Spange on the occasion of his 60th birthday

Abstract: Triethoxysilyl functionalized phenothiazinyl ureas were synthesized and immobilized by in situ synthesis into mesoporous hybrid materials. The designed precursor molecules influence the structure of the final materials and the intermolecular distance of the phenothiazines. XRD and N₂ adsorption measurements indicate the presence of

highly ordered two-dimensional hexagonally structured functional materials, while the incorporation of the organic

Keywords: electron transfer · mesoporous materials · optical materials · organic–inorganic hybrid composites · phenothiazine

compounds in the solid materials was proved by means of ¹³C and ²⁹Si solid state NMR spectroscopy as well as by FT-IR spectroscopy. Upon oxidation with (NO)BF₄ or SbCl₅, stable phenothiazine radical cations were generated in the pores of the materials, which was detected by means of UV/Vis, emission, and EPR spectroscopies.

Introduction

Since the discovery of mesoporous silicas in 1992,^[1,2] research on these materials has rapidly developed. They can be readily obtained by the micellar condensation of silicic acid derivatives. The pores of such solids can be used for different applications.^[2,3] Chemical and physical manipulation of the outer and the inner surface as well as in the bulk material have been reported.^[4] One of the main areas of research in this field is related to applications in catalysis.^[5] However, because of pore sizes in the range of 2–30 nm, these solids have also been used for the stabilization of nanoparticles (quantum dots),^[6] for the synthesis of nanowires,^[7] or magnetic and optic materials.^[8] Adsorption of reactive species at the walls of those materials was used for stabilization, almost similar to the isolation in the cavities of zeolites. This idea was, for example, adopted to stabilize photochromic dyes in mesoporous materials,^[9] to stabilize and organize chlorophyll a in order to mimic the energy transfer and charge separation of photosynthesis,^[10] to heterogenize VO²⁺ and cytochrome c for oxygen activation,^[11] to investigate the photoinduced charge separation of pyrene^[12] and to stabilize benzene radicals in the mesopores of phenyl substituted MCM-41.^[13]

Phenothiazines that represent nitrogen and sulfur containing heterocycles^[14] have gained different applications, such

[a] Dr. Z. Zhou, A. Wagener, Prof. Dr. S. Ernst, Prof. Dr. W. R. Thiel
Fachbereich Chemie
Technische Universität Kaiserslautern
Erwin-Schrödinger-Str. Geb. 54, D-67663 Kaiserslautern (Germany)
Fax: (+49)631-2054676
E-mail: thiel@chemie.uni-kl.de

[b] Dr. A. W. Franz, S. Bay, Prof. Dr. T. J. J. Müller
Institut für Organische Chemie und Makromolekulare Chemie
Heinrich Heine Universität Düsseldorf
Universitätsstr. 1, D-40225 Düsseldorf (Germany)
Fax: (+49)211-8114324
E-mail: ThomasJJ.Mueller@uni-duesseldorf.de

[c] Dr. B. Sarkar
Institut für Anorganische Chemie
Universität Stuttgart
Pfaffenwaldring 55, D-70569 Stuttgart (Germany)

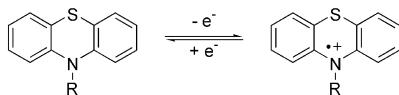
[d] Dr. A. Seifert
Institut für Chemie
Technische Universität Chemnitz
Strasse der Nationen 62, D-09107 Chemnitz (Germany)

[e] Dr. P. Yang
College of Materials Science and Chemical Engineering
Harbin Engineering University
Harbin 150001 (China)

[f] Dr. M. Pagels
Schlumberger Cambridge Research
High Cross, Madingley Road, Cambridge, CB3 0EL (UK)

Supporting information for this article is available on the WWW under <http://dx.doi.org/10.1002/asia.201000098>.

as in pharmaceuticals.^[15] An important feature of the phenothiazine motif is a reversible one-electron oxidation process with a low potential that leads to stable and deep colored radical cations, as shown in Scheme 1.^[16]



Scheme 1. The reversible one-electron oxidation process of the phenothiazine motif.

Consequently, phenothiazine derivatives have found application in materials sciences as electrophoric sensors in supramolecular systems for photoinduced electron transfer (PET)^[17] and as electron donors in electronically conducting charge-transfer composites.^[18] Furthermore, phenothiazine polymers obtained by polycondensation play an important role, for example, as electrochromic materials for displays.^[19] On the other hand, the low oxidation potential of polyphenothiazines is responsible for its capability to act as an electron donor in fluorescent donor–acceptor chromophores, which are of special use as emitters in organic light-emitting diodes (OLED)^[20,21] as well as for nonlinear optical and electrooptical effects.^[22]

The generation of efficient devices requires not only the control of the electronic but also of the spatial properties of a given system. It has been shown, for example, that the electronic properties of π -conjugated materials strongly depend on the interaction of the molecules and, thus, on their intermolecular orientation.^[23] From this point of view, it appears to be beneficial to combine the properties of periodically ordered inorganic mesoporous materials (strong orientation of the pore system) and phenothiazines (electrooptic features) for a rational design of one-dimensionally stacked redox active molecules. To date, there are only a few reports on the physisorption of phenothiazines on silica, presumably because of the weak forces between the aromatic molecules and the silica surface,^[24] which hampers the formation of stable materials. It has been shown by means of EPR spectroscopy that phenothiazine physisorbed on porous silicas can form stable radical cations by photooxidation, where the silica network might act as an electron acceptor.^[25] Doping the support with transition metal ions or using transition metal oxides as the support facilitates the electron transfer process.^[26] Furthermore, chlorinated hydrocarbons can be used as electron acceptors,^[25] a most favorable aspect for the photochemical degradation of persistent and ecotoxic compounds.

In a previous work, we introduced phenothiazines by covalent grafting on mesoporous MCM-41 and SBA-15 host structures.^[27] Although post-synthetic grafting is the most popular way to anchor organic groups in a specific manner to a silica surface, which finally results in organic–inorganic hybrid materials, there are still some drawbacks related to

this procedure. First of all, the distribution of the organic groups is generally not uniform within one channel, and secondly, the loading with larger and sterically demanding organic functionalities is often low, mainly constrained by diffusion limitations. Therefore, in order to increase the phenothiazine content in the pores and for the exploration of the properties of these materials, such as intermolecular charge transfer, an alternative method, providing a high content of the electroactive chromophores and thus enabling intermolecular electron transfer over a longer distance, was envisioned. Hence, we decided to prepare the mesoporous hybrid materials by a template-directed synthesis in the presence of siloxylated phenothiazines. In this strategy, the siloxane precursors act as building blocks for the construction of the main framework, whereas the organosiloxanes contribute to both the silicate framework units and the organic functional groups on the surface. This one-step synthesis can produce mesoporous solids with a high loading of organic functional groups and a homogeneous surface coverage within the channels of the materials. During the gelation process, the organic moieties are supposed to extend into the micelle causing an intramolecular phase separation. Thus, the rational design of the organic precursors, which must additionally be stable under the conditions of the materials synthesis, is of utmost importance. Here, we report the synthesis and properties of urea-linked phenothiazines, as well as their transformation into organic/inorganic mesoporous materials by in situ synthesis, which results in a high and uniform phenothiazine loading. In addition to their structures, their electronic properties will also be presented.

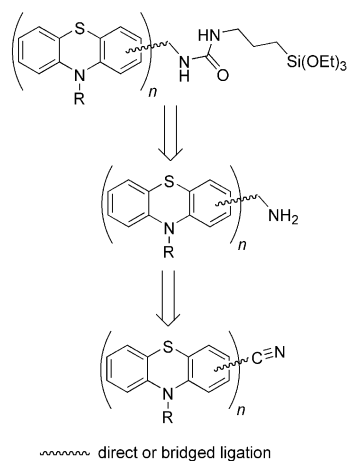
Results and Discussion

Synthesis and Properties of Urea-linked Triethoxysilylated Phenothiazines

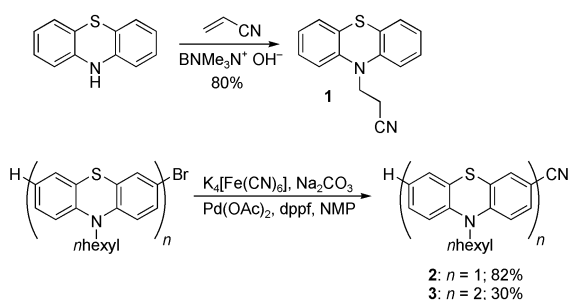
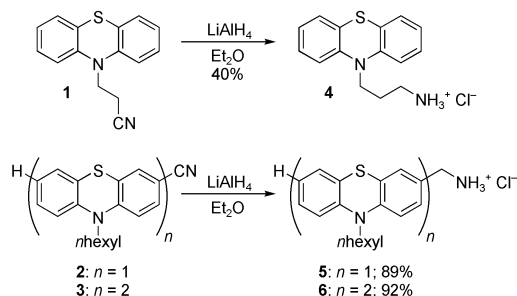
Ureas are synthesized by the straightforward addition of an amine to an isocyanate. The major advantage of this approach lies in its highly atom-economical use of both the starting materials that react almost quantitatively without the formation of any by-products. Therefore, the retrosynthetic analysis of urea-based phenothiazinyl building blocks for their incorporation in mesoporous silica suggests the formation of urea from a phenothiazinyl substituted amine with a triethoxysilyl functionalized isocyanate (Scheme 2). The amine in turn is readily accessible by reduction of the corresponding phenothiazinyl cyano compound.

The phenothiazinyl nitrile **1** is easily prepared by Michael addition of acrylonitrile to 10*H*-phenothiazine,^[28] and the cyano compounds **2** and **3** with extended π -conjugation are obtained by Beller cyanation^[29] in moderate to good yields (Scheme 3).^[30]

Upon standard reduction with lithium aluminium hydride in refluxing diethyl ether, the cyano compounds **1–3** were readily reduced to give the corresponding amines as amine hydrochlorides **4–6** in moderate to good yields (Scheme 4). With these amine hydrochlorides in hand, the stage was set

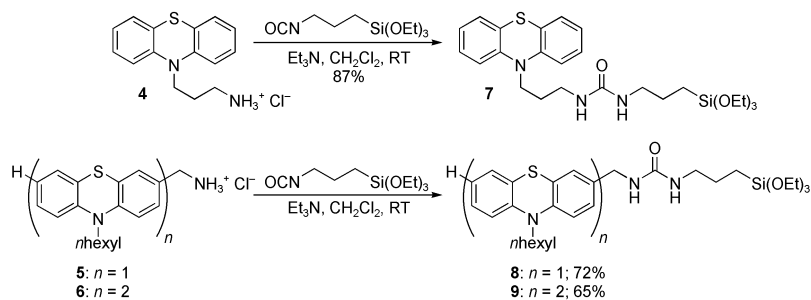


Scheme 2. Retrosynthetic analysis of urea-based phenothiazinyl building blocks.

Scheme 3. Synthesis of (oligo)phenothiazinyl cyano derivatives **1–3**.Scheme 4. Reduction of **1–3** with LiAlH_4 to the corresponding amines **4–6**.

for the introduction of the triethoxysilane linker by isocyanate addition.

The amine hydrochlorides **4–6** were reacted in the presence of triethylamine with 3-(triethoxysilyl)propylisocyanate in dry dichloromethane at 40°C under an argon atmosphere and the corresponding ureas **7–9** were obtained in good to excellent yields (Scheme 5). The structures of the ureas were un-

Scheme 5. Synthesis of triethoxysilyl functionalized (oligo)phenothiazine ureas **7–9**.

ambiguously supported by ^1H and ^{13}C NMR spectroscopies, mass spectrometry, and correct combustion analyses or high resolution mass spectrometry.

In contrast to the previously reported carbamates,^[27] urea linked trialkoxysilyl functionalized compounds **7–9** reveal some special properties. First, urea groups are inherently able to form hydrogen bonds (vide infra). This interesting property can be applied to assemble molecules into well-defined supramolecular architectures^[31] or to control the morphology of the hybrid materials.^[32] In addition, urea groups can interact effectively with anionic species by hydrogen bonding.^[33] Based upon this feature, several sensors with urea as the functional group have been reported.^[34] For instance, by linking a urea group to a fluorescent unit, these molecules become suitable for detection of anionic species by reverse photoinduced electron transfer (PET) by causing a decrease in fluorescence intensity. Furthermore, urea has frequently been used in the past for the generation of organosilicas.^[35] Therefore, urea-based linkers were chosen to induce a pre-organization of the phenothiazine moieties by intermolecular hydrogen bonds in the micelle formation, which leads to a stacked arrangement of the heteroaromatic rings. Upon transfer into the final hybrid material as suggested by Figure 1, facilitated electronic interaction could be

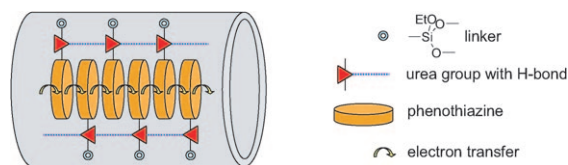


Figure 1. An idealized illustration of the intermolecular electron transfer between the phenothiazines.

anticipated. Another important aspect of the urea group is its chemical and thermal stability. As mentioned before, for the one-pot co-condensation synthesis of hybrid mesoporous materials, a robust and firm organic precursor, which can sustain under strong acidic and basic conditions, remains a prerequisite. The electron donor/acceptor system in the confined channel of mesoporous silica materials will ultimately be formed upon partial oxidation.

Table 1. Selected absorption and emission spectra^[a] and cyclic voltammetry^[b] data of the (oligo)phenothiazine ureas **7–9** and of the mesoporous hybrid materials **10–12**.

compound	absorption $\lambda_{max,abs}$ [nm] (ϵ)	emission $\lambda_{max,em}$ [nm]	Stokes shift $\Delta\bar{\nu}$ [cm^{-1}]	$E_0^{0/+1}$ [mV]
7	257 (47100), 310 (7200)	449, 511 (sh.)	10000	690
8	260 (20300), 314 (3100)	459	10000	669
9	267 (79000), 323 (30000)	458	9100	595, 761
10-1	250, 304	436	10000	–
10-2	251, 307	438	9800	671 ^[c]
10-3	248, 305	388 (sh), 437	9900	720 ^[c]
11-1	256, 308	388, 450	10300	–
11-2	255, 311	456	10200	–
11-3	255, 310	378, 437	9400	–
12-1	255, 310	436	9900	–
12-2	268, 324	467, 512 (sh)	9500	–

[a] Recorded in CH_2Cl_2 , $T=20^\circ\text{C}$; [b] Recorded in CH_2Cl_2 , $T=20^\circ\text{C}$, $\nu=100\text{ mV s}^{-1}$, electrolyte: $(n\text{Bu}_4\text{N})\text{PF}_6$, Pt working electrode, Pt counter electrode, Ag/AgCl reference electrode. [c] Recorded in CH_3CN , $T=20^\circ\text{C}$, $\nu=100\text{ mV s}^{-1}$, electrolyte: $(n\text{Bu}_4\text{N})\text{PF}_6$, Pt working electrode, Pt counter electrode, Ag/AgCl reference electrode.

The electronic properties of the phenothiazine ureas **7–9** have been investigated by absorption and emission spectroscopy and by cyclic voltammetry (Table 1). The most characteristic absorption of ureas in the UV region (two distinct bands at 260 and 310 nm) is accompanied by a blue to greenish blue fluorescence (broad unstructured bands with a maximum at 450 nm and occasionally a shoulder at 510 nm) for all representatives. With 10000 cm^{-1} , the Stokes shifts are quite remarkable and can be attributed to significant geometrical changes upon excitation for many phenothiazine derivatives from a highly non-planar ground state to a largely planarized excited state.^[36] Electrochemical data for the presented phenothiazines were obtained by cyclic voltammetry in the anodic region (up to 1.5 V). The first oxidation potentials stemming from the most electron rich phenothiazine core were found in the range from $E_0^{0/+1}=595\text{ mV}$ (diphenothiazine **9**) to $E_0^{0/+1}=690\text{ mV}$ (monophenothiazine **7**) (Figure 2).

Synthesis and Properties of Urea-linked Phenothiazine/MCM-41 Hybrid Materials

The urea unit is sufficiently stable to allow the co-condensation of the phenothiazinyl derivatives with tetraethoxysilane (TEOS) in the presence of the base EtNH_2 at 100°C and prolonged reaction times. The main feature of this synthetic route is the usage of EtNH_2 instead of the conventionally applied strong base NaOH , thus avoiding the incorporation of Na^+ ions into the mesoporous materials.^[37] Under the given conditions, MCM-41 type mesoporous materials featuring a uniform two dimensional hexagonal channels was formed. The pore size of these materials can easily be settled between 2 to 3 nm by using CTAB as the template, which provides an ideal matrix for the different phenothiazine units. To obtain a uniform distribution of the phenothiazine and to avoid phase separation during the formation of the mesoporous structure, TEOS and **7** (or **8**, **9**) were first dissolved in a small volume of methanol prior to the ad-

dition of this mixture to the surfactant solution. A slow dropwise addition of this mixture to the surfactant solution is important. The addition of a certain amount of methanol in the synthesis of MCM-41 can increase the degree of order of the mesoporous structure compared with a purely aqueous system.^[38,39] For comparison, the same method was used for the synthesis of pure silica MCM-41. After template extraction with EtOH/HCl under reflux conditions, the well-ordered MCM-41 hybrid materi-

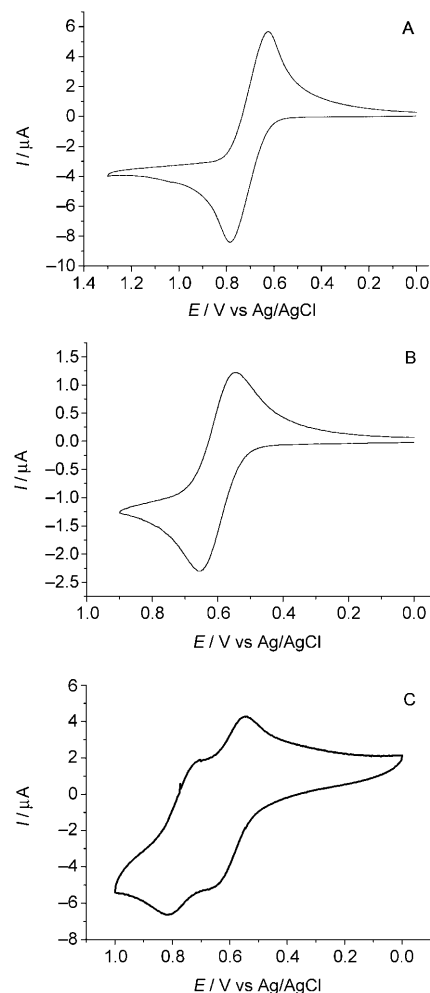
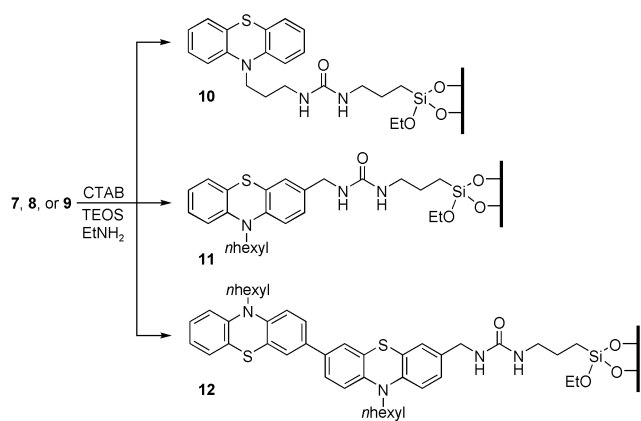


Figure 2. A: cyclic voltammogram of **7**; B: cyclic voltammogram of **8** ($n\text{Bu}_4\text{N}^+\text{PF}_6^-/\text{CH}_2\text{Cl}_2$, 20°C , $\nu=100\text{ mV s}^{-1}$, Pt-working electrode, Pt-counter electrode, Ag/AgCl reference electrode); C: cyclic voltammogram of **9**; ($n\text{Bu}_4\text{N}^+\text{PF}_6^-/\text{CH}_2\text{Cl}_2$, 20°C , $\nu=250\text{ mV s}^{-1}$, Pt-working electrode, Pt-counter electrode, Ag/AgCl reference electrode).



Scheme 6. In situ synthesis of the mesoporous hybrid materials **10**, **11**, and **12** with CTAB as the template.

als **10–12** were obtained (Scheme 6). To determine the influence of the concentration and molecular structure of phenothiazine on the configuration of the hybrid mesoporous materials, various concentrations and well-designed phenothiazine moieties were employed (Table 2).

Table 2. Textural parameters of the hybrid materials **10**, **11**, and **12** derived from nitrogen adsorption–desorption analysis or powder X-ray diffraction and loading of phenothiazines in the hybrid materials.

sample	$d_{100}^{[a]}$ [nm]	$a_0^{[b]}$ [nm]	$S_{\text{BET}}^{[c]}$ [$\text{m}^2 \text{g}^{-1}$]	$V_p^{[d]}$ [$\text{cm}^3 \text{g}^{-1}$]	$D_p^{[e]}$ [nm]	$w_t^{[f]}$ [nm]	$C^{[g]}$ [mol %]	content of phenothiazine ^[h]	
								[mmol g^{-1}]	[wt %]
MCM-41	4.30	4.96	1123	0.98	2.83	2.14	–	–	–
10-1	4.38	5.06	1040	0.85	2.48	2.58	17.8	0.33	13.0
10-2	4.23	4.88	914	0.69	2.41	2.48	35.0	0.54	21.2
10-3	4.20	4.85	700	0.42	2.25	2.60	53.6	0.77	30.2
11-1	4.05	4.68	991	0.78	2.65	2.02	15.7	0.26	11.7
11-2	4.00	4.62	766	0.58	2.68	1.94	26.4	0.40	17.9
11-3	3.98	4.60	638	0.51	2.69	1.90	37.1	0.54	24.2
12-1	4.04	4.66	761	0.65	2.64	2.02	18.6	0.28	20.4
12-2	3.96	4.57	632	0.57	2.58	1.98	25.7	0.35	25.2

[a] d_{100} : $d(100)$ spacing. [b] $a_0 = 2d_{100}/\sqrt{3}$. [c] S_{BET} : BET surface area. [d] V_p : Pore volume. [e] D_p : Pore diameter. [f] w_t : Wall thickness ($a_0 - D_p$). [g] Molar ratio of precursor/CTAB. [h] Calculated from the nitrogen content (CHN analysis).

Structural Characterization and Properties of the Hybrid Materials

Powder X-ray Diffraction

Powder XRD was carried out to elucidate the structural ordering of the mesoporous materials. For comparison, neat MCM-41 was synthesized and analyzed. The powder XRD patterns of all materials are given in the Supporting Information. Generally, all samples exhibited typical reflections of a material possessing two-dimensional hexagonal $p6mm$ symmetry.^[1b,40] The intensity of the reflections was found to increase after the extraction of the template CTAB, which can be assigned to an enhancement of the contrast density between the framework and pore channels.^[41] For neat MCM-41, an increase in the d_{100} spacing from 4.27 to 4.30 nm was observed. This can be attributed to an ongoing condensation of silicon species in the material framework

during the template extraction process.^[42] The textural parameters of all the hybrid materials are summarized in Table 2. Exemplarily, the XRD patterns of the compounds **10** with different amounts of phenothiazine (**10-1**: 0.33; **10-2**: 0.54; **10-3**: 0.77 mmol g^{-1}) are shown in Figure 3.

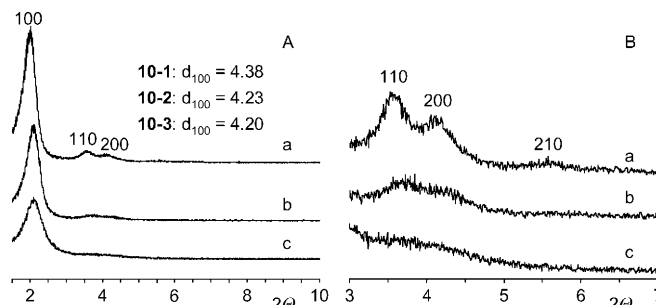


Figure 3. A: Powder XRD pattern of compounds **10**; a) **10-1**, b) **10-2**, and c) **10-3**. B: magnified signals at $3^\circ < 2\theta < 7^\circ$.

Compound **10-1** showed four Bragg diffraction peaks similar to MCM-41, which indicated a long-range ordered hexagonal mesostructure. The d_{100} value (4.38 nm) increased slightly compared to neat MCM-41, presumably caused by an increased micelle diameter at the given concentration.^[43] The characteristic (100) peak shifts slightly to larger 2θ values at higher concentrations of precursor **7**, which corresponds to a decrease in the d spacing (**10-2**: 4.23; **10-3**: 4.20 nm). In these cases, **7** significantly expels the surfactant in the hydrophobic

phase during the formation of the micelles.^[44] This disturbs the surfactant cooperation with the inorganic species by balanced Coulomb interactions to form micelles fully covered with silica species. Therefore, the unit cell will contract after the hydrothermal reaction.^[45] Parallel to the increase of the phenothiazine content, the relative intensities of all diffraction peaks decrease, particularly the peaks at higher angles. For **10-3**, the second order peaks (110) and (200) are overlapping, and the peak of the (210) plane is nearly undetectable. This feature may partially be attributed to a decrease in the mesoscopic order of the materials, and partially because of the contrast matching between the amorphous silicate framework and organic moieties which are located inside the channels.^[5d,43,44,46] While the samples **11-1**, **11-2**, and **11-3** show a similar influence of the phenothiazine concentration on the XRD pattern and on the cell parameters (see Supporting Information), the biphenothiazine series, **12-1** and

12-2, are different. The XRD pattern of **12-1** (0.28 mmol of biphenothiazine per g) presents a normal peak pattern with clearly detectable (100), (110), (200), and (210) reflections typical for two-dimensional hexagonal $p6mm$ symmetry (see Supporting Information). Compound **12-2** shows an intense (100) peak and a peculiar intense (200) peak overlapping the (110) peak. This indicates the formation of a distorted hexagonal structure or an intermediate phase between a hexagonal and a lamellar configuration.^[47,48] In the literature, this has been explained with a distorted hexagonal structure, which might be because of the amorphous nature of the mesoporous silica framework.^[49] The silica species in this type of structural materials have a wide range of Si–O–Si bond angles, which are much more flexible than in crystalline zeolites.^[50] We assign this behaviour to the large molecular structure of precursor **9**, which could disturb not just the micelles but also the final structure of the silica framework to some degree. The presence of a transition phase can be traced back to the classical surfactant pair packing parameter, $g = V/a_0l$, in which a variation of g can be indexed to phase transitions and different geometries of the mesophase products.^[50] For **12-2**, the high content of **9** would dramatically increase the hydrophobic volume V , and thus the value of g is increased, which results in a decrease of surface curvature and thus in a mesophase transition between the hexagonal and the lamellar structure.^[51,52]

N_2 Adsorption/Desorption

The nitrogen adsorption isotherms for the extracted phenothiazine-urea functionalized hybrid materials are all presented in the Supporting Information, and the corresponding data are listed in Table 2. All the eight samples display typical IV isotherms (definition by IUPAC),^[53] with a sharp capillary condensation step in the low P/P_0 range of 0.2 to 0.4, which confirms the ordered mesoporous structure of these materials. In this region, only compound **10-1** exhibited a narrow hysteresis loop in the steep low-pressure region, which may be because of nitrogen occupying the regions between adjacent organic groups and the silica wall.^[43,54] A further narrow H4 type hysteresis loop observed for **10-1** and **10-2** on the horizontal portion (from P/P_0 0.45–0.95) can be linked to uniform slit-shaped pores.^[55,56]

Generally, quite narrow pore size distributions are observed, which demonstrates the presence of uniform pores. In combination with the increase of organic material in the samples, the volume of total adsorption continuously decreases, which can be attributed to a decline in the surface area and the total pore volume. For the samples **10**, the position of the capillary condensation step gradually shifts from a relative pressure of ~ 0.24 to ~ 0.19 , which indicates a systematic decrease of the pore size,^[57] which as expected corroborates with the decrease of the d_{100} values and the unit cell parameter a_0 determined by XRD (see above). For the samples **11**, completely reversible isotherms and the absence of any hysteresis loops, indicate ordered mesoporous materials with uniform pore sizes and ordered arrangements of cylindrical channels without any intersecting disorder.^[58] Here,

the pore size distribution curves indicate a slight increase of the pore size, which is in contrast to the situation discussed for the samples **10**. This could be related to the process of the mesostructure formation. The behavior of samples **12** is again different. Here, a second inflection appears at P/P_0 close to 0.42–1, which displays a H4-type hysteresis loop in the desorption branch of the isotherm. This feature is characteristic of slit-like pores, which may be the result of textural porosity within the particles or because of an intersecting disorder of the materials.^[55]

By analyzing the textural parameters summarized in Table 2, a general conclusion can be deduced. The d_{100} spacings, the specific BET surface areas, and the pore volume are reduced with increased amounts of organic silane in the reaction mixture. A similar behavior was observed by others who investigated the loading with pendent organic groups by applying the co-condensation method.^[59,60,61] An increase in the pore filling organic component decreases the pore volume and the specific surface areas, which is easily understandable, whilst the reasons for a decrease in d_{100} spacing upon increase of the organic precursor concentration are not so easily understood. Some studies ascribe this trend to different interactions between the cationic surfactant molecules and the silicate or organosilicate precursors during the hydrothermal reaction.^[43,62] In our case, the reaction mixtures leading to **10**, **11**, and **12** contain organosilicates with different phenothiazine fragments, which could influence the process of the mesophase formation. In this process, inorganic species and organic molecules will interact. The micelle interface curvature depends on Coulomb attraction/repulsion, van der Waals interactions, hydrogen bonds, and covalent bonds between inorganic/organic units.^[45,63] The synthesis of **10**, **11**, and **12** was performed at pH ~ 13 , while the aqueous isoelectric point (IEP) of the silica species was at pH ~ 2 .^[64] Therefore, the silicate species are negatively charged, and will interact with the positively charged surfactant head groups by Coulomb attraction. The inorganic species/organic surfactant interface will thus be influenced by the location and concentration of the phenothiazine precursor, which again would be influenced by the molecular size and shape of the phenothiazinyl substituted silanes. During the micelle formation, the siloxane group of the precursor will be embedded in the inorganic layer, while the phenothiazine group might be located near this interface or reach the internal core depending on the molecular geometry of the precursor.^[64]

In the case of **7**, the phenothiazine core should be located closer to the interface, which results in the reduction of the silanol groups in this region. Thus, less surfactant molecules are required for charge balance, which leads to a remarkable contraction of the cylindrical micelle size in the hybrid materials with increasing precursor concentrations. In contrast, compound **8** bears the urea linker in the 3-position and the hexyl chain in the 10-position. This molecular structure is favorable for interaction with the template molecules through hydrophobic interactions. Therefore, the phenothiazine group will be drawn further into the inner part of the

surfactant micelles and the influence of the concentration of **8** on the interface layer will not be as significant as in the case of **7**.

Electron Microscopy

Transmission electron microscopy (TEM) is an indispensable tool for the characterization of the hybrid materials. It provides direct evidence for the structural ordering of the materials in the form of images, and helps in the direct discovery of intrinsic pore structures of hybrid materials.^[65] TEM and SEM images of all samples are included in the Supporting Information. The mesostructure depends on the concentration and the molecular structure of the precursor in the reaction mixture. Especially the hybrid materials **10-1** and **11-1** show uniform and highly ordered structures. Consistent with the XRD results, an increase in the precursor concentration slightly reduces the ordering of the materials. The mesostructure changes significantly for the diphenothiazine derived system **12-2**. While **12-1** still exhibits hexagonally arranged pore channels, **12-2** presents a certain type of nanofilament elongated specifically along the channel direction of the hybrid mesostructure. Based on TEM (Figure 4) and XRD data, an explanation for the formation of this

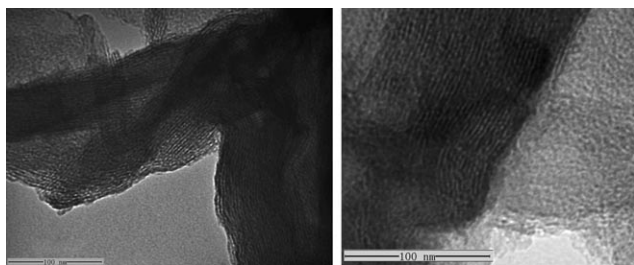


Figure 4. TEM images of the hybrid mesoporous material **12-2**.

structure can be proposed. The large hydrophobic biphenothiazine precursor **9** can undergo π - π interaction and the parallel molecules can protract vertical to the cross-section of the micelles. Hence, long tubular-type micelles can be expected, which is in accordance with the extremely long channels observed by TEM and the distorted transition structure derived from the XRD data.

Obviously, differences in the microscopic regime during the gelation process will also have an influence on the macroscopic morphology of the products.^[66,67] This can also be found for the phenothiazine modified hybrid materials, although most of the observed morphologies are not as uniform as reported for certain examples in the literature. This is because of our synthetic process, which includes a long hydrothermal treatment. However, this is favourable for the complete hydrolysis of the silica species and for achieving a high loading of organic moieties. Powdery products are obtained rather than morphologically uniform nanoscale materials. SEM pictures of all samples are included in the Supporting Information.

FT-IR Spectroscopy

The infrared absorptions of the N-H and the C=O groups in urea are quite sensitive to hydrogen bonding.^[68] In solution, intermolecular hydrogen bonding is concentration dependent, that is, the higher the concentration of the sample, the greater the extent of hydrogen bonding.^[69] We used this feature to determine the interaction of the urea-linked phenothiazines in the organic/inorganic hybrid materials.

First, the concentration dependence of the IR spectra of precursor **7** was studied in a CH_2Cl_2 solution. Figure 5 pres-

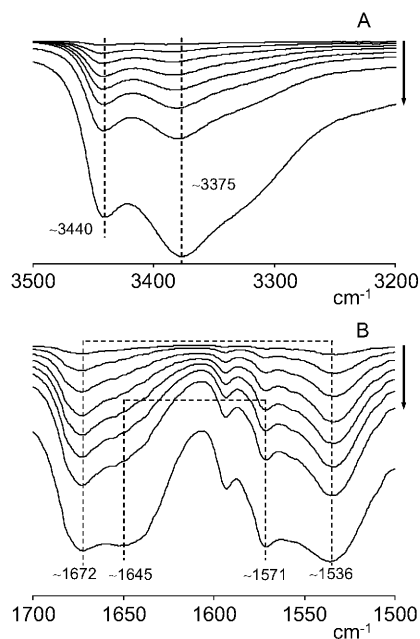


Figure 5. FT-IR spectra of **7** in CH_2Cl_2 ; concentrations: 2.0, 6.0, 12.0, 18.0, 24.0, 30.0, 36.0, 50.0 mmolL^{-1} .

ents the concentration dependence of $\nu_{\text{N-H}}$ and the amide I ($\nu_{\text{C=O}}$) and the amide II band ($\delta_{\text{N-H}}$)^[69] of precursor **7** in CH_2Cl_2 solution. The $\nu_{\text{N-H}}$ at around 3440 cm^{-1} is typical for free ureas and the $\nu_{\text{N-H}}$ at about 3375 cm^{-1} can be assigned to hydrogen bonding urea groups.^[68] Obviously, this band increased with increasing concentration, and simultaneously, the center of this band shifted slightly to lower wavenumbers and an additional shoulder at around 3325 cm^{-1} was observed at the highest concentration. Hydrogen bonding weakens the C=O bond and thus leads to a decrease of the stretching frequency. Therefore, the $\nu_{\text{C=O}}$ at around 1672 cm^{-1} can be assigned to free urea groups and the band at about 1645 cm^{-1} to the intermolecular hydrogen bonded urea groups. Similarly $\delta_{\text{N-H}}$ was also observed as two bands at about 1536 and 1571 cm^{-1} . The absorption at lower wavenumbers corresponds to free urea groups, and the absorption at higher wavenumbers to urea units involved in intermolecular hydrogen bonds. A decrease in $\Delta\nu$ (amide I – amide II) was clearly observed and is in agreement with

dominant hydrogen bonding urea groups in nonpolar organic media.^[70]

Figure 6 (spectrum a) shows the absorbance of the neat precursor **7**. Comparison with the solution spectra indicates that the peak at 3440 cm⁻¹, characteristic for free urea groups, has disappeared. Additionally, a significant shift of

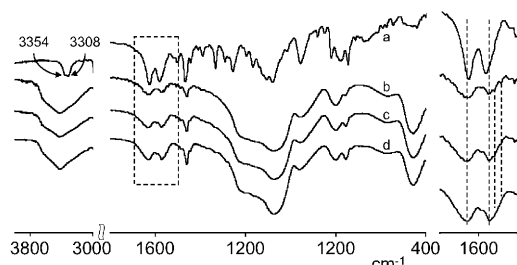


Figure 6. FT-IR spectrum (KBr) of a) **7**, b) **10-1**, c) **10-2**, and d) **10-3** (right side inset: amide I and amide II bands).

the signals assigned to hydrogen bound urea groups^[68,69] from 3375 cm⁻¹ in solution to 3354 and 3308 cm⁻¹ in the solid state could be observed, which indicates at least two different types of N–H bonds. Furthermore, strong absorptions were found for $\nu_{C=O}$ and δ_{N-H} . In neat solid **7**, $\nu_{C=O}$ was found at 1625 cm⁻¹ and δ_{N-H} at 1580 cm⁻¹. Both bands are redshifted compared to the solution data, which is in agreement with a higher degree of intermolecular hydrogen bonding in the solid state. Furthermore, $\Delta\nu$ is significantly smaller (45 cm⁻¹) than for free urea groups (120 cm⁻¹)^[70] and even smaller than the $\Delta\nu$ of precursor **7** in solution (74 cm⁻¹). All these observations can be correlated to a strong association of urea groups by hydrogen bonding in the solid state.

The IR spectra of **10-1**, **10-2**, and **10-3** are also shown in Figure 6. They are typical for all hybrid materials discussed in this manuscript (see the Supporting Information) and shall be discussed exemplarily here. Generally a broad absorption is observed in the range of 3600–3200 cm⁻¹, which can be assigned to the ν_{OH} stretching vibration of the hydrogen-bound silanol groups.^[71] Further broad bands at 1300–1100 cm⁻¹ are attributed to the asymmetric vibration of the Si–O–Si units of the silica network. The absorption at 955 cm⁻¹ derives from the stretching vibration of the surface Si–O groups, and the peak at 800 cm⁻¹ is attributed to the symmetric vibration of Si–O–Si. A strong absorption at 460 cm⁻¹ is assigned to the bending vibration of Si–O–Si.^[72] In addition to these signals typical for silica, some further absorptions can be assigned to the organic moieties. The stretching vibration of aliphatic C–H groups appears at around 2980–2850 cm⁻¹ (not shown in Figure 6) and the absorption at 1470 cm⁻¹ arises from the C–H deformation vibration. The typical urea ν_{N-H} vibration is covered by the Si–OH vibrations. However, the characteristic $\nu_{C=O}$ and δ_{N-H} absorptions can be observed at ~1629 cm⁻¹ and ~1572 cm⁻¹,

respectively. The corresponding $\Delta\nu$ is 55 cm⁻¹, which is in fact a little larger than the value found for neat **7** ($\Delta\nu$ = 45 cm⁻¹), but still much smaller than for free urea ($\Delta\nu$ = 120 cm⁻¹). This indicates the presence of hydrogen-bound urea groups in the hybrid materials. Furthermore, the low loading samples **10-1** (0.33 mmol g⁻¹) and **10-2** (0.54 mmol g⁻¹) present two small peaks around 1542 and 1558 cm⁻¹, which disappear in the high loading sample **10-3** (0.77 mmol g⁻¹). This implies a higher degree of hydrogen bonding in the latter sample, which can be assigned to larger aggregates of phenothiazines interacting through hydrogen bonds.

For neat **9**, the $\Delta\nu$ value (58 cm⁻¹) still indicates hydrogen bond interactions, although it is significantly larger than for neat **7** (44 cm⁻¹) and **8** (43 cm⁻¹). This may be attributed to the two phenothiazine groups in **9** which will hamper the interaction of the urea groups by increased steric hindrance. In the IR spectra of the hybrid materials **12**, a series of $\nu_{C=O}$ and δ_{N-H} vibrations indicated differently bound urea units.

The most significant IR data of the precursors **7–9** and the hybrid materials **10–12** are summarized in Table 3. Generally, the $\Delta\nu$ values of the neat organic ureas are smaller than those found for the hybrid materials, which indicates that intermolecular hydrogen bond interactions are decreased in these materials. This phenomenon can be easily rationalized, because the average distance of molecules in the hybrid materials should be larger than in the pure precursor.

Table 3. IR data of the precursors **7–9** and the hybrid materials **10–12**.

sample	ν_{N-H}	$\nu_{C=O}$	δ_{N-H}	$\Delta\nu$ (min, max) ^[a]	n [nm ²]	d [nm]
7	3354 3308	1625	1580	45	–	–
10-1	–	1628	1573 1558	55 70	0.19	2.27
10-2	–	1628	1573 1558	55 70	0.36	1.68
10-3	–	1628	1573	55	0.66	1.23
8	3308	1620	1577	43	–	–
11-1	–	1645	1576 1559 1543	60 102	0.16	2.51
11-2	–	1645	1576 1559 1543	60 102	0.31	1.80
11-3	–	1645	1576 1559 1543	60 102	0.51	1.40
9	3358	1633	1575	58	–	–
12-1	–	1645	1574 (sh) 1568 1559 1542	62 103	0.22	2.12
12-2	–	1645	1574 (sh) 1568 1559 1542	62, 103	0.33	1.73

[a] $\Delta\nu$ = amide I – amide II ($\Delta\nu_{min}$ = amide I_{min} – amide II_{max}, and $\Delta\nu_{max}$ = amide I_{max} – amide II_{min}).

Solid State NMR Spectroscopy

^{13}C CP-MAS NMR spectroscopy provides information on the integration of the organic component in the hybrid materials. As an example, the spectrum of **10-2** is shown in Figure 7, with dashed lines representing the resonances of

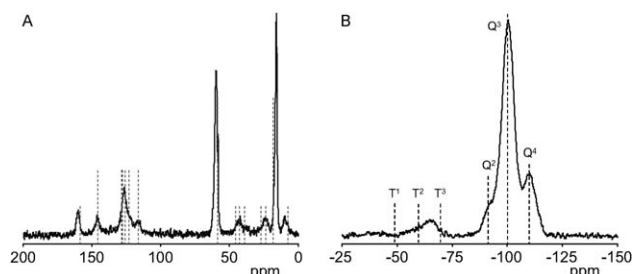


Figure 7. A) ^{13}C CP-MAS NMR and B) ^{29}Si CP-MAS NMR spectrum of **10-2**; the dashed lines in the ^{13}C NMR spectrum give information on the position and the relative intensities of the resonances in the solution ^{13}C NMR spectrum of **7**.

precursor **7** in solution (for the solid state ^{13}C NMR spectra of all other hybrid materials, see the Supporting Information). Obviously, the resonances of the solid state material are quite similar compared to the solution spectrum. The resonance at $\delta = 7.6$ is assigned to the carbon atom bound to silicon, which confirms that there is no cleavage of the C–Si bond during the synthesis. Two sharp peaks at $\delta = 16$ and 60 are assigned to the residual Si–OCH₂CH₃ groups. The resonance at $\delta = \sim 40$ can be assigned to the carbon atoms bound to the urea unit, which demonstrates the stability of the urea group under the co-condensation conditions. Several signals in the low field region ($\delta = \sim 130$ – 114) are typical for an electron rich aromatic system and can be assigned to the carbon nuclei of the phenothiazine core. Compared to the spectrum obtained in solution, a small shift of the resonance of the C=O group ($\delta = \sim 158$) to lower field is ascribed to hydrogen bonding of the urea group.

Solid state ^{29}Si CP-MAS NMR spectra provide information on the silicon environment and the degree of organic functionalization. Figure 7 shows the ^{29}Si CP-MAS NMR spectrum of **10-2** (for the solid state ^{29}Si NMR spectra of all other hybrid materials, see the Supporting Information). A peak of low intensity ($\delta = -92$) corresponds to geminal (HO)₂Si(SiO)₂ (Q²) sites while the most intense resonance of the spectrum ($\delta = -101$) is assigned to isolated (HO)Si(SiO)₃ (Q³) silanol sites. A further resonance in this region ($\delta = -110$) is ascribed to Si(SiO)₄ (Q⁴) centers and completes the characterization of the silica bulk material.^[73] Usually three signals at $\delta = -49$, -59 , and -69 can be assigned to organo silicon species R–Si(HO)₂(OSi) (T¹), R–Si(HO)(OSi)₂ (T²), and RSi–(OSi)₃ (T³), respectively.^[74] Here, a broad band centered at $\delta = -65$ was observed, which means that the major Si–C species are of the T² and T³ type. This indicates quite a complete cross-linking be-

tween the phenothiazine precursor **7** and TEOS during the co-condensation process.^[75]

Electronic and Optical Properties of the Hybrid Materials

All hybrid material samples **10-1**, **10-2**, and **10-3** were characterized by solid state cyclic voltammetry. The powdered hybrid materials were abrasively immobilized on a glassy carbon electrode and the cyclic voltammograms were recorded in acetonitrile solution with 0.1 M *n*Bu₄N⁺PF₆[−] as supporting electrolyte. Figure 8 shows a series of cyclic voltammograms obtained from **10-3** with varying scan rates (see the Supporting Information for the data of **10-1** and **10-2**).

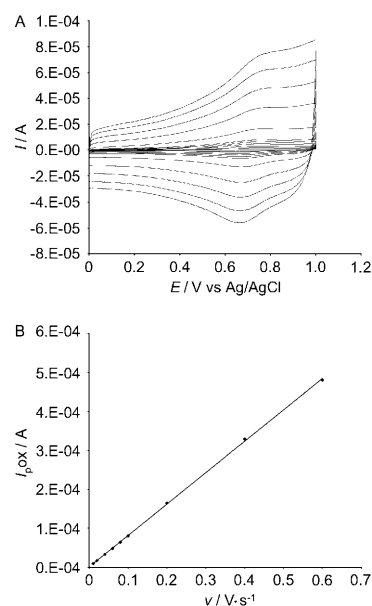


Figure 8. A) Cyclic voltammograms with varying scan rates (0.01, 0.02, 0.04, 0.06, 0.08, 0.10, 0.20, 0.40, 0.60, 0.80, 1.00 V s^{−1}) of an electrode modified with **10-3** (0.1 M (*n*Bu₄N)PF₆, CH₃CN, RT). B) Plot of oxidation peak currents versus scan rates, linear regression analysis gives: $y = 8 \cdot 10^{-5}x + 1 \cdot 10^{-7}$, $R^2 = 0.9997$.

A potential sweep with a **10-3** modified GC electrode at a scan rate of 0.1 V s^{−1} reveals an oxidation wave at a potential of 762 mV and a reduction wave at a potential of 678 mV against Ag/AgCl. The half-wave potential of this reversible one electron transfer is 720 mV, with a peak separation of 84 mV. Variation of the scan rate in the range of 0.01–1.0 V s^{−1} still gives reversible redox signals with the peak potentials being fairly constant, and the peak currents increasing with increasing scan rate.

There are two possible pathways to realize the electron transfer in these hybrid mesoporous materials.^[76] One is a direct electron transfer from the electrochemically active species to electrode surface, which would require pronounced mobility of the redox sites. This mechanism is usually observed for redox active sites physically adsorbed in mesoporous materials.^[77] A second possible mechanism is a

long-range electron transfer by the immobilized redox active sites to the electrode surface through electron exchange between adjacent redox centers (electron hopping).^[78,79] Since in **10-3**, the electrochemical active centers (phenothiazines) are covalently fixed in the pores of the mesoporous silica matrix, the latter mechanism obviously appears to be more plausible. Further evidence for electron hopping is presented in Figure 8 (bottom), where the oxidation peak currents are plotted against the scan rates showing a linear relationship. This also indicates surface bound redox centers.^[77] In a multi-sweep experiment, **10-3** showed high stability (see the Supporting Information). After 100 scans, the overall current just slightly decreased, probably because of mechanical loss of the powdery material from the electrode surface. This is different from a diffusion controlled electrochemical reaction with a supported material on the electrode. In that case, the current should decrease quickly, owing to diffusion of redox active species into the electrolyte.^[77,80]

The UV/Vis spectra of the hybrid material samples **10-1**, **10-2**, and **10-3** are illustrated in Figure 9 (for the UV/Vis spectra of all other hybrid materials, see the Supporting Information, characteristic data are summarized in Table 1).

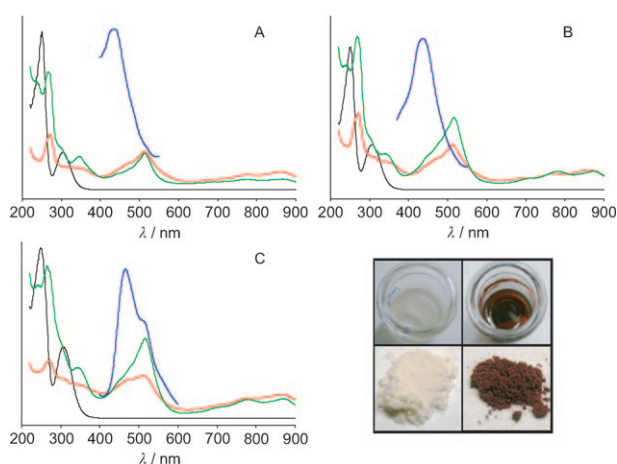


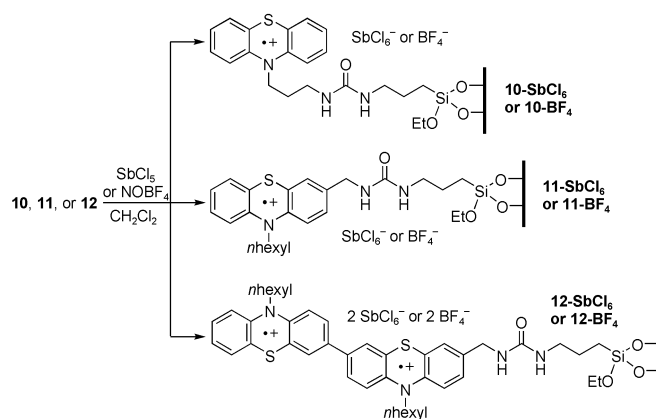
Figure 9. UV/Vis spectra (black lines) of **10-1** (A), **10-2** (B) and **10-3** (C) of the corresponding radical cationic samples **10-1-BF₄**, **10-2-BF₄**, **10-3-BF₄** (red lines), **10-1-SbCl₆**, **10-2-SbCl₆**, **10-3-SbCl₆** (green lines) and emission spectra of **10-1**, **10-2**, and **10-3** (blue lines). The inset picture demonstrates the color change caused by the oxidation of **10-1** using NOBF₄ in suspension and for the corresponding solid.

The three samples present two absorptions in the UV. Compared to the spectrum of precursor **7** in CH₂Cl₂, a slight hypsochromic shift of the absorption maxima can be observed for the hybrid materials, which can be attributed to the interactions between the silica surface and the phenothiazine core or a consequence of a one-dimensional H-type aggregation of phenothiazine molecules in the channel of the mesoporous material (H-aggregate, face-to-face arrangement).^[81,82] A change in the phenothiazine content causes no shift of the absorption maxima. Only a slight broadening of

the bands can be considered with an increased loading of phenothiazine (see the Supporting Information), which may be attributed to weak π -electron interactions with surface bound Si–OH groups,^[83] or may be a result of H-aggregation, which usually is accompanied with a further hypsochromic shift.^[36,82,84,85]

Figure 9 also shows the emission spectra of **10-1**, **10-2**, and **10-3** (blue lines). All the emissions were located at ~ 437 nm, which had shifted hypsochromically compared to the data of **7** in CH₂Cl₂ solution (peak maximum: 449 nm; shoulder: 511 nm). The Stokes shift is ~ 10000 cm⁻¹. Interestingly, a second emission could be observed in the spectra of **10-2** (small shoulder) and **10-3** (shoulder: ~ 515 nm). As already discussed for the absorption of the samples **10-1**, **10-2**, and **10-3**, aggregation also affects the luminescence by a substantial blue shift of the emission bands, presumably caused by π -stacking, which is essentially absent in solution. Therefore the silanol groups on the surface of the materials would have a strong influence on such TICT states.

The hybrid materials undergo formation of surface bound radical cations when treated with oxidizing agents (Scheme 7). Oxidation was carried out with the one-electron



Scheme 7. Oxidation of the mesoporous phenothiazinyl hybrid materials.

oxidants SbCl₅ and NOBF₄ in CH₂Cl₂ suspension, leaving SbCl₆⁻ and BF₄⁻ as the counter ions, respectively. For the materials **10-1**, **10-2**, and **10-3**, a color change to red was observed during the oxidation reaction (Figure 9, inset). This color change manifests in an absorption band around 515 nm typical for phenothiazine radical cations. Additionally, a broad absorption band in the NIR region could be observed. The intensity of these bands increases with increasing loading of phenothiazine. Such NIR bands have often been associated with a charge resonance transition of cofacially oriented aromatic donor/acceptor dyads.^[86] It is also well known that electron transfer between the phenothiazine moiety and its radical cation can occur.^[16c,d] Furthermore, these NIR bands are absent in monophenothiazine modified mesoporous materials obtained by post synthetic grafting.^[27b] Thus, we assign this NIR bands to an intermolecular charge transfer (CT), which demonstrates that the

co-condensation method is an appropriate way to achieve strongly intermolecularly coupled phenothiazine complexes.

It is worthwhile to mention that the resulting deeply colored materials retain their color under ambient temperature for several weeks when stored under an atmosphere of dry nitrogen, which indicates high stability of the radical cations in the mesoporous hybrid materials. The red color fades to pink when the materials are exposed to air at room temperature for 3 days. The absorption spectra of these exposed materials are shown in the Supporting Information. The typical absorptions of the phenothiazine radical cations are still present in the absorption spectrum but with decreased intensity. Compared to the freshly generated materials, a novel and intense peak at 344 nm was detected, which might be associated with a new compound generated by a phenothiazine radical cation consuming reaction that leads to the corresponding S-oxide through disproportionation of the radical cation.^[87]

While the hybrid materials **11-1**, **11-2**, and **11-3** show UV/Vis data similar to the compound **10** series, the materials **12-1** and **12-2** derived from the diphenothiazine precursor **9** behave differently. Oxidation of **12-1** and **12-2** by strongly oxidizing SbCl_5 furnished dark greenish products with an absorption spectrum, which was different to those of the monophenothiazine radical cations discussed above, indicating the presence of complex dicationic species.^[16b,c]

EPR Spectroscopy

Electron paramagnetic resonance was used to additionally confirm the existence of the stable phenothiazine radical cations in the hybrid materials. The EPR spectrum of **12-2-SbCl₆** is shown in Figure 10. It reveals a g-value of 2.0053

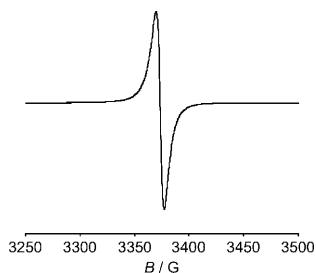


Figure 10. Q-band EPR spectrum of **12-2-SbCl₆** at 297°C.

typical for phenothiazine radical cations. Since the EPR signal was not well resolved, hyperfine coupling constants and anisotropic g-tensors could not be determined. However, the high symmetry of the EPR spectrum indicates that the phenothiazine radicals are in an isotropic environment in the hybrid material.

Conclusions

Novel hybrid organic/inorganic mesoporous silica materials were synthesized by covalently anchoring phenothiazines on

MCM-41 following an in-situ methodology. The highly ordered hexagonal mesoporous structures of the materials were confirmed by XRD and N_2 adsorption measurements. ^{13}C CP-MAS, ^{29}Si CP-MAS NMR, and FT-IR data exhibit the successful incorporation of the organic species into the solid materials. The existence of stable phenothiazine radical cations in the materials has been clearly detected by UV/Vis and EPR spectroscopy. In our ongoing project, we are working to increase the phenothiazine content in the pores. This could lead to systems that exhibit charge transfer properties or even electronic conductivities.

Experimental Section

General

All manipulations were carried out under an inert atmosphere of nitrogen and the solvents were dried by standard methods. Reagents were purchased and used without further purification, unless otherwise noted.

Reagent grade reagents, catalysts, and solvents were purchased and used without further purification. THF, diethyl ether, and methylene chloride were dried and distilled according to standard procedures.^[88] The phenothiazine nitriles **2** and **3** were prepared according to literature procedures.^[30] Column chromatography: silica gel 60, mesh 70–230. TLC: silica gel plates. ^1H and ^{13}C NMR spectra: CD_2Cl_2 , CDCl_3 , and $[\text{D}_6]$ acetone (locked to Me_4Si).^[89] The assignments of quaternary C, CH, CH_2 , and CH_3 have been made by DEPT spectra. Elemental analyses were carried out in the Microanalytical Laboratories of the Organisch-Chemisches Institut, Ruprecht-Karls-Universität, Heidelberg, Germany, in the Microanalytical Laboratories of the Institut für Pharmazeutische Chemie, Heinrich-Heine-Universität, Düsseldorf, Germany and in the Analytical Laboratory of the Fachbereich Chemie, Technische Universität Kaiserslautern, Kaiserslautern, Germany.

Electrochemistry

Cyclic voltammetry experiments (EG&G potentiostatic instrumentation) were performed under argon in dry and degassed CH_2Cl_2 at room temperature and at scan rates of 100, 250, 500, and 1000 mVs^{-1} . The electrolyte was Bu_4NPF_6 (0.025 M). The working electrode was a 1 mm platinum disk, the counter-electrode was a platinum wire, and the reference electrode was a Ag/AgCl electrode. The potentials were corrected to the internal standard of Fc/Fc^+ in CH_2Cl_2 ($E_0^{0/+1} = 450 \text{ mV}$).^[90]

Infrared spectra (KBr) were recorded using a Jasco FT-IR-6100 spectrometer. X-ray powder diffraction (XRD) patterns were obtained on a Siemens D5005 diffractometer with $\text{Cu}_{\text{K}\alpha}$ radiation (30 kV, 30 mA). Nitrogen adsorption and desorption isotherms were measured at 77 K on a Quantachrome Autosorb 1 sorption analyzer after evacuation of the samples at 120°C overnight. The specific surface areas were calculated by the Brunauer-Emmett-Teller (BET) equation in the low relative pressure interval (< 0.3) and the pore size distribution curves were analyzed with the adsorption branch by the BJH method. ^{13}C CP MAS and ^{29}Si CP MAS NMR were carried out on a Bruker DSX Avance spectrometer at resonance frequencies of 100.6 and 79.5 MHz, respectively. UV/Vis diffuse reflectance spectra were recorded on a Perkin-Elmer Lambda-18 with neat-MCM-41 as the background standard. Q-band CW ESR experiments have been performed at 297 K on a Bruker EMX 10–40 spectrometer.

Synthesis

3-(10H-phenothiazine-10-yl)propionitrile (1): 10H-phenothiazine (10.0 g, 50.0 mmol) was suspended in acrylonitrile (75 mL, 1.13 mol) and cooled to 0°C. Triton B (5 mL) was added slowly and carefully to the well-stirred suspension, and then the reaction mixture was allowed to warm up to room temperature. The solution was diluted with 1,4-dioxane (100 mL) and stirred for 1 h at 101°C. After cooling to RT, the solution was

poured into water and a light brown solid precipitated. The solid was filtered off and dried in vacuo. Recrystallization from acetone gave **1** (10.0 g, 80%) as colorless crystals. M.p.: 156°C (lit.: 156–157°C);^[28] ¹H NMR (CD₂Cl₂, 500 MHz): δ = 2.84 (t, *J* = 7.0 Hz, 2H), 4.23 (t, *J* = 7.0 Hz, 2H), 6.87 (d, *J* = 8.0 Hz, 2H), 6.99 (dt, ¹*J* = 7.5 Hz, ⁴*J* = 1.0 Hz, 2H), 7.21 ppm (m, 4H); ¹³C NMR (CD₂Cl₂, 125 MHz): δ = 16.2 (CH₂), 43.0 (CH₂), 115.1 (CH), 117.2 (C_{quat.}), 123.0 (CH), 125.8 (C_{quat.}), 127.2 (CH), 127.4 (CH), 143.7 ppm (C_{quat.}); MS (EI⁺): *m/z* (%): 252.0 (73, *M*⁺), 212.0 (100, *M*⁺ - CH₂CN), 198.0 (71, *M*⁺ - (CH₂)₂CN), 180.1 (71); elemental analysis: calcd (%) for C₁₅H₂₂N₂S (252.2): C 71.40, H 4.79, N 11.10; found: C 71.11, H 5.03, N 11.70.

General procedure for the reduction of phenothiazine substituted cyano compounds 1–3 with lithium aluminium hydride (GP1): A solution of the phenothiazine substituted cyano compounds **1–3** (1 equiv) in dry diethyl ether was slowly added, through a dropping funnel, to a well-stirred mixture of lithium aluminium hydride (2.3 equiv per CN bond) in dry diethyl ether heated to 40°C, over 20–30 min. The reaction mixture was stirred at 40°C for 16 h and was then cooled to 0°C. Then, water (50 mL) and diluted aqueous sodium hydroxide solution (20 wt %, 10 mL) were added. The precipitate was filtered and the aqueous phase was washed with small portions of diethyl ether. A small portion of conc. hydrochloric acid was added to the combined organic phases and the orange or red precipitated products **4–6** were filtered and dried in vacuo.

3-(10*H*-phenothiazine-10-yl)propylamine hydrochloride (4): **1** (2.94 g, 11.7 mmol) was placed in a Soxhlet extractor and was extracted into dry diethyl ether (500 mL) containing lithium aluminium hydride (1.02 g, 26.9 mmol). The extraction was performed at 40°C for 3 d after which the mixture was decomposed by means of addition of water (1 mL) and 20% aqueous sodium hydroxide solution (6 mL). The salts were removed by filtration and the amine hydrochloride was isolated by the addition of conc. hydrochloric acid (1 mL) into the ethereal filtrate. Compound **4** was obtained as colorless needles (1.66 g, 48%). M.p.: 227°C; ¹H NMR ([D₆]DMSO, 500 MHz): δ = 2.00 (t, *J* = 7.25 Hz, 2H), 2.87 (m, 2H), 3.99 (t, *J* = 6.8 Hz, 2H), 6.97 (t, *J* = 7.5 Hz, 2H), 7.08 (d, *J* = 8.0 Hz, 2H), 7.20 (m, 4H), 8.15 ppm (br, 3H); ¹³C NMR ([D₆]DMSO, 125 MHz): δ = 24.5 (CH₂), 36.5 (CH₂), 43.6 (CH₂), 116.0 (CH), 122.6 (CH), 123.9 (C_{quat.}), 127.1 (CH), 127.6 (CH), 144.5 ppm (C_{quat.}); MS (FAB⁺): *m/z* (%): 257.2 (100, *M*⁺), 256.2 (70, *M*⁺ - H), 212.2 (23, *M*⁺ - (CH₂)₂NH₂), 199.2 (22, *M*⁺ - (CH₃)₂NH₂); elemental analysis: calcd (%) for C₁₅H₁₆N₂S·HCl (257.3+35.5): C 61.52, H 5.85, N 9.57; found: C 61.29, H 5.93, N 9.33.

(10-Hexyl-10*H*-phenothiazine-3-yl)methylamine hydrochloride (5): According to GP1, the amine hydrochloride **5** (3.14 g, 89%) was isolated as a light yellow solid. M.p.: 46°C; IR (film): $\tilde{\nu}$ = 2925, 1578, 1493, 1463, 1377, 1334, 1243, 1133, 887, 819, 746 cm⁻¹; ¹H NMR ([D₆]DMSO, 500 MHz): δ = 0.81 (t, *J* = 7.0 Hz, 3H), 1.22 (m, 4H), 1.36 (m, 2H), 1.65 (m, 2H), 3.86 (t, *J* = 7.0 Hz, 2H), 3.90 (m, 2H), 6.94 (t, *J* = 7.5 Hz, 1H), 7.02 (d, *J* = 7.5 Hz, 2H), 7.14 (dd, *J* = 1.5 Hz, *J* = 7.5 Hz, 1H), 7.20 (t, *J* = 7.0 Hz, 1H), 7.29 (m, 2H), 8.33 ppm (br, 3H); ¹³C NMR ([D₆]DMSO, 125 MHz): δ = 13.8 (CH₃), 22.0 (CH₂), 25.7 (CH₂), 26.1 (CH₂), 30.8 (CH₂), 41.3 (CH₂), 46.4 (CH₂), 115.6 (CH), 115.9 (CH), 122.6 (CH), 123.0 (C_{quat.}), 123.6 (C_{quat.}), 127.1 (CH), 127.7 (CH), 127.8 (CH), 128.0 (C_{quat.}), 128.5 (CH), 144.5 (C_{quat.}), 144.8 ppm (C_{quat.}); MS (FAB⁺): *m/z* (%): 312.3 (73, *M*⁺), 296.0 (100, *M*⁺ - NH₂), 241.2 (8, *M*⁺ - C₅H₁₁), 227.1 (11, *M*⁺ - C₆H₁₃), 212.1 (17), 211.1 (12, *M*⁺ - NH₂ - C₆H₁₃); elemental analysis: calcd (%) for C₁₉H₂₄N₂S·HCl (312.3+36.5): C 65.40, H 7.22, N 8.03; found: C 65.20, H 7.18, N 7.96.

(10,10'-Dihexyl-10*H*,10'*H*-3',3'-biphenothiazine-3-yl)methylamine hydrochloride (6): According to GP1 the amine hydrochloride **6** (689 mg, 92%) was isolated as a yellow solid. M.p.: 152°C; UV/Vis (CH₂Cl₂): λ_{max} (ε): 270 (88500), 284 (73600), 325 nm (32700); IR (KBr): $\tilde{\nu}$ = 2926, 2854, 1603, 1578, 1460, 1415, 1375, 1333, 1245, 1193, 1106, 1054, 873, 807, 746, 613 cm⁻¹; ¹H NMR ([D₆]DMSO, 500 MHz): δ = 0.81 (m, 6H), 1.22–1.36 (m, 12H), 1.66 (m, 4H), 2.49 (s, 2H) 3.85 (m, 6H), 6.92–7.12 (m, 4H), 7.14–7.41 (m, 8H), 8.28 ppm (s, 2H); ¹³C NMR ([D₆]DMSO, 125 MHz): δ = 14.0 (CH₃), 22.2 (CH₂), 26.4 (CH₂), 31.1 (CH₂), 46.6 (CH₂), 47.8 (CH₂), 115.7 (CH), 115.9 (CH), 116.2 (CH), 116.3 (CH), 122.6 (CH), 123.3 (C_{quat.}), 123.4 (C_{quat.}), 123.7 (C_{quat.}), 124.3 (C_{quat.}), 124.5 (CH),

124.5 (CH), 125.3 (CH), 125.4 (CH), 127.3 (CH), 127.8 (CH), 127.9 (CH), 128.2 (C_{quat.}), 128.7 (CH), 133.2 (C_{quat.}), 133.5 ppm (C_{quat.}); MS (MALDI): calcd (%) for C₃₇H₄₃N₃S₂: 593.290; found: 593.162.

General procedure for the synthesis of the urea-linked triethoxysilylated phenothiazines 7–9 (GP2): In a heat gun dried Schlenk vessel, the amine hydrochlorides **4–6** (1 equiv) were suspended in dry dichloromethane (0.04 M) under nitrogen and triethylamine (2 equiv) was added. Upon stirring for 30 min at RT, the suspension dissolved and the color changed from orange to yellow. Then, 3-(triethoxysilyl)propylisocyanate (1 equiv) was slowly added to the reaction mixture and the reaction was monitored by TLC. After 2 h, the solvent was removed in vacuum. The crude product was absorbed on celite and chromatographed on silica gel (hexanes/ethyl acetate = 2:3). The urea-linked triethoxysilylated phenothiazines **7–9** were obtained as pure yellow solids.

(10*H*-phenothiazine-10-yl)propyl-3-(triethoxysilyl)propylurea (7): Yield: 87%. ¹H NMR (CDCl₃, 600 MHz): δ = 0.58 (t, *J* = 8.4 Hz, 2H), 1.24 (t, *J* = 7 Hz, 9.0H), 1.52 (m, 2H), 2.00 (m, 2H), 3.02 (q, *J* = 6 Hz, 2H), 3.30 (q, *J* = 6 Hz, 2H), 3.82 (q, *J* = 7.2 Hz, 6H), 3.99 (t, *J* = 6 Hz, 2H), 4.46 (br, 1H), 4.90 (br, 1H), 6.93–6.99 (m, 4H), 7.19 ppm (m, 4H); ¹³C NMR (CDCl₃, 150.92 MHz): δ = 7.6 (CH₂), 18.3 (CH₃), 23.6 (CH₂), 26.7 (CH₂), 39.0 (CH₂), 42.8 (CH₂), 45.4 (CH₂), 58.4 (CH₂), 116.0 (CH), 122.9 (C), 125.4 (CH), 127.6 (CH), 127.8 (CH), 145.3 (C), 158.2 ppm (C=O); elemental analysis: calcd (%) for C₂₅H₃₇N₃O₄SSi (503.73): C 59.61, H 7.40, N 8.34; found: C 59.10, H 7.51, N 8.20.

(10-hexyl-10*H*-phenothiazine-3-yl)methyl-3-(triethoxysilyl)propylurea (8): Yield: 72%. ¹H NMR (CDCl₃, 400 MHz): δ = 0.60 (t, *J* = 8.2 Hz, 2H), 0.86 (t, *J* = 6.8 Hz, 3H), 1.21 (t, *J* = 7 Hz, 9.0H), 1.27–1.31 (m, 4H), 1.41 (m, 2H), 1.60 (m, 2H), 1.77 (m, 2H), 3.14 (m, 2H), 3.70–3.87 (m, 8H), 4.15 (m, 2H), 4.80 (br, 1H), 4.92 (br, 1H), 6.7–6.9 (m, 3H), 7.0–7.2 ppm (m, 4H); ¹³C NMR (CDCl₃, 150.92 MHz): δ = 7.9 (CH₂), 14.3 (CH₃), 18.7 (CH₃), 22.9 (CH₂), 24.0 (CH₂), 27.0 (CH₂), 31.8 (CH₂), 43.3 (CH₂), 44.1 (CH₂), 47.8 (CH₂), 58.8 (CH₂), 115.7 (CH), 115.9 (CH), 122.6 (CH), 125.0 (C), 126.9 (C), 127.6 (CH), 127.8 (CH), 133.9 (CH), 144.8 (C), 145.6 (C), 158.6 ppm (C=O); elemental analysis: calcd (%) for C₂₉H₄₅N₃O₄SSi (559.84): C 62.22, H 8.10, N 7.51; found: C 61.60, H 7.98, N 7.20.

(10,10'-dihexyl-10*H*,10'*H*-3',3'-biphenothiazine-7-yl)methyl-3-(triethoxysilyl)propylurea (9): Yield: 65%. ¹H NMR (CDCl₃, 400 MHz): δ = 0.62 (t, *J* = 8.0 Hz, 2H), 0.86 (t, *J* = 7.0 Hz, 6H), 1.21 (t, *J* = 7 Hz, 9H), 1.27–1.31 (m, 8H), 1.40 (m, 4H), 1.61 (m, 2H), 1.75 (m, 4H), 3.14 (m, 2H), 3.71–3.90 (m, 10H), 4.14 (m, 2H), 5.41 (br, 1H), 5.25 (br, 1H), 6.65 (d, *J* = 6, 1H), 6.71 (d, *J* = 6, 1H), 6.81 (m, 4H), 7.01 (m, 2H), 7.12 (m, 1H), 7.19–7.27 ppm (m, 4H); ¹³C NMR (CDCl₃, 150.92 MHz): δ = 7.6 (CH₂), 14.0 (CH₃), 18.3 (CH₃), 22.6 (CH₂), 23.6 (CH₂), 26.6 (CH₂), 26.7 (CH₂), 31.5 (CH₂), 42.9 (CH₂), 43.5 (CH₂), 47.5 (CH₂), 58.4 (CH₂), 114.3 (CH), 115.2 (CH), 115.3 (CH), 115.6 (CH), 116.4 (CH), 122.3 (CH), 124.4 (C), 125.0 (CH), 125.1 (CH), 126.5 (CH), 126.6 (CH), 127.2 (CH), 127.4 (CH), 129.5 (CH), 129.9 (C), 133.7 (C), 133.8 (C), 134.5 (C), 143.7 (C), 144.2 (C), 158.7 ppm (C=O); elemental analysis: calcd (%) for C₄₇H₆₄N₄O₄S₂Si (841.25): C 67.10, H 7.67, N 6.66; found: C 66.60, H 7.98, N 6.40.

General procedure for the synthesis of the hybrid materials: In a typical synthetic procedure, an aqueous solution of CTAB was mixed with ethylamine under stirring. Then a solution of the precursor **7**, **8**, or **9** in methanol and an appropriate amount of TEOS were added dropwise. The composition of the mixture in molar ratio was 1.0:x:0.14:2.4:2.0:100 SiO₂/precursor/CTAB/EtNH₂/methanol/H₂O (**10-1**: x = 0.025, **10-2**: x = 0.049, **10-3**: x = 0.075, **11-1**: x = 0.022, **M2-2**: x = 0.037, **11-3**: x = 0.052, **12-1**: x = 0.026, **M3-2**: x = 0.036). The reaction mixture was stirred for a further 24 h at RT before being heated to 100°C for 24 h. The product was recovered by filtration, washed thoroughly with distilled water until pH 7 was achieved. The colorless powdery material was dried in vacuum at 50°C. The surfactant (CTAB) was extracted by twofold stirring of the as-synthesized hybrid material (1.0 g) in ethanol (80 mL) and an aqueous solution of HCl (36%, 1.0 mL) under reflux for 8 h. The resulting solid was then filtered, washed with ethanol and CH₂Cl₂ and vacuum dried at 50°C. Elemental analyses: **10-1**: C 11.68, H 2.05, N 1.37, corresponding to a loading of 0.33 mmol g⁻¹; **10-2**: C 16.53, H 2.83, N 2.26, corresponding to a loading of 0.54 mmol g⁻¹; **10-3**: C 20.33, H 2.81, N 3.25, corresponding to a loading of 0.77 mmol g⁻¹; **11-1**: C 10.16, H 2.60, N 1.10, corresponding to

a loading of 0.26 mmol g⁻¹; **11-2**: C 17.79, H 3.23, N 1.68, corresponding to a loading of 0.40 mmol g⁻¹; **11-3**: C 19.81, H 3.59, N 2.25, corresponding to a loading of 0.54 mmol g⁻¹; **12-1**: C 15.24, H 2.40, N 1.54, corresponding to a loading of 0.28 mmol g⁻¹; **12-2**: C 19.79, H 2.97, N 1.93, corresponding to a loading of 0.34 mmol g⁻¹.

Generation of radical cations: In a typical process, the hybrid material (0.10 g) was suspended in dry dichloromethane (5 mL). The solution was stirred at RT and a molar excess of NOBF₄ or SbCl₅ was added. The color of the samples immediately changed. The solids were filtered off, extracted with dichloromethane, and dried under vacuum.

Acknowledgements

This project was supported by the DFG Schwerpunktprogramm SPP 1181 (Nanoscaled Inorganic Materials by Molecular Design: New Materials for Advanced Technologies; NANOMAT).

- [1] a) C. T. Kresge, M. E. Leonowicz, W. J. Roth, J. C. Vartuli, J. S. Beck, *Nature* **1992**, 359, 710–712; b) J. S. Beck, J. C. Vartuli, W. J. Roth, M. E. Leonowicz, C. T. Kresge, K. D. Schmitt, C. T. W. Chu, D. H. Olson, E. W. Sheppard, S. B. McCullen, J. B. Higgins, J. L. Schlenker, *J. Am. Chem. Soc.* **1992**, 114, 10834–10843.
- [2] a) G. J. de A. A. Soler-Illia, C. Sanchez, B. Lebeau, J. Patarin, *Chem. Rev.* **2002**, 102, 4093–4138; b) M. Widenmeyer, R. Anwander, *Chem. Mater.* **2002**, 14, 1827–1831.
- [3] a) H.-P. Lin, C.-Y. Mou, *Acc. Chem. Res.* **2002**, 35, 927–935; b) B. Hatton, K. Landskron, W. Whitnall, D. Perovic, G. A. Ozin, *Acc. Chem. Res.* **2005**, 38, 305–312.
- [4] a) R. Anwander, *Chem. Mater.* **2001**, 13, 4419–4438; b) J. Morell, G. Wolter, M. Fröba, *Chem. Mater.* **2005**, 17, 804–808; c) C. Yoshina-Ishii, T. Asefa, N. Coombs, M. J. MacLachlan, G. A. Ozin, *Chem. Commun.* **1999**, 2539–2540; d) S. Guan, S. Inagaki, T. Ohsuna, O. Terasaki, *J. Am. Chem. Soc.* **2000**, 122, 5660–5661; e) S. Inagaki, S. Guan, Y. Fukushima, T. Ohsuna, O. Terasaki, *J. Am. Chem. Soc.* **1999**, 121, 9611–9614; f) B. J. Melde, B. T. Holland, C. F. Blanford, A. Stein, *Chem. Mater.* **1999**, 11, 3302–3308; g) T. Asefa, M. J. MacLachlan, N. Coombs, G. A. Ozin, *Nature* **1999**, 402, 867–871; h) J. Sauer, F. Marlow, B. Spliethoff, F. Schüth, *Chem. Mater.* **2002**, 14, 217–224; i) T. Abe, Y. Tachibana, M. Iwamoto, *Chem. Commun.* **1995**, 1617–1618; j) H. van Bekkum, K. R. Kloetstra, *Stud. Surf. Sci. Catal.* **1998**, 117, 171–182; k) V. R. Choudhary, S. K. Jana, B. P. Kiran, *J. Catal.* **2000**, 192, 257–261; l) M. Iwamoto, T. Abe, Y. Tachibana, *J. Mol. Catal. A* **2000**, 155, 143–153; m) A. Wingen, N. Anastasievic, A. Hollnagel, D. Werner, F. Schüth, *J. Catal.* **2000**, 193, 248–254; n) M. Fröba, R. Köhn, G. Bouffaud, O. Richard, G. van Tendeloo, *Chem. Mater.* **1999**, 11, 2858–2865; o) A. Zecchina, D. Scarano, G. Spoto, S. Bordiga, C. Lamberti, G. Bellussi, *Stud. Surf. Sci. Catal.* **1998**, 117, 343–350; p) F. Hoffmann, M. Cornelius, J. Morell, M. Fröba, *Angew. Chem.* **2006**, 118, 3290–3328; *Angew. Chem. Int. Ed.* **2006**, 45, 3216–3251; q) A. Stein, B. J. Melde, R. C. Schroden, *Adv. Mater.* **2000**, 12, 1403–1419.
- [5] a) D. E. de Vos, M. Dams, B. F. Sels, P. A. Jacobs, *Chem. Rev.* **2002**, 102, 3615–3640; b) A. P. Wight, M. E. Davis, *Chem. Rev.* **2002**, 102, 3589–3614; c) C. E. Song, S. Lee, *Chem. Rev.* **2002**, 102, 3495–3524; d) A. Sayari, S. Hamoudi, *Chem. Mater.* **2001**, 13, 3151–3168.
- [6] a) R. Plass, S. Pelet, J. Krüger, M. Grätzel, U. Bach, *J. Phys. Chem. B* **2002**, 106, 7578–7580; b) X. Gao, S. Nie, *J. Phys. Chem. B* **2003**, 107, 11575–11578.
- [7] F. J. Brieler, P. Grundmann, M. Fröba, L. Chen, P. J. Klar, W. Heimbrot, H.-A. Krug von Nidda, T. Kurz, A. Loidl, *J. Am. Chem. Soc.* **2004**, 126, 797–807.
- [8] a) F. J. Brieler, P. Grundmann, M. Fröba, L. Chen, P. J. Klar, W. Heimbrot, H.-A. Krug von Nidda, T. Kurz, A. Loidl, *Chem. Mater.* **2005**, 17, 795–803; b) A.-H. Lu, W.-C. Li, A. Kiefer, W. Schmidt, E. Bill, G. Fink, F. Schüth, *J. Am. Chem. Soc.* **2004**, 126, 8616–8617.
- [9] S. A. Song, G. R. Lee, S. H. Lim, H. M. Kim, S. B. Park, S. M. Yang, *Repub. Korean Kongkai Taeho Kongbo* **2008**, KR 2008004237.
- [10] T. Itoh, K. Yano, T. Kajino, S. Itoh, Y. Shibata, H. Mino, R. Miyamoto, Y. Inada, S. Iwai, Y. Fukushima, *J. Phys. Chem. B* **2004**, 108, 13683–13687.
- [11] a) C.-H. Lee, T.-S. Lin, C.-Y. Mou, *J. Phys. Chem. B* **2003**, 107, 2543–2551; b) C.-H. Lee, J. Lang, C.-W. Yen, P.-C. Shih, T.-S. Lin, C.-Y. Mou, *J. Phys. Chem. B* **2005**, 109, 12277–12286.
- [12] a) K. T. Ranjit, L. Kevan, *J. Phys. Chem. B* **2003**, 107, 2610; b) R. M. Krishna, L. Kevan, *Phys. Chem. Chem. Phys.* **2001**, 3, 5348–5353.
- [13] K. Toriyama, M. Okazaki, *Phys. Chem. Chem. Phys.* **1999**, 1, 2607–2612.
- [14] a) M. Sainsbury in *Rodd's Chem. Carbon Compd.*, Vol. 4, 2nd ed., (Ed.: M. Sainsbury), Elsevier, Amsterdam, **1998**, p. 575; b) M. Sainsbury in *Comprehensive Heterocyclic Chemistry*, Vol. 3, (Eds.: A. R. Katritzky, C. W. Rees), Pergamon Press, Oxford, **1984**, p. 995; c) H. J. Shine, D. R. Thompson, C. J. Veneziani, *Heterocycl. Chem.* **1967**, 4, 517–527; d) L. A. Tinker, A. J. Bard, *J. Am. Chem. Soc.* **1979**, 101, 2316–2319; e) B. Paduszek, M. K. Kalinowski, *Electrochim. Acta* **1983**, 28, 639–642.
- [15] a) F. Mietzsch, *Angew. Chem.* **1954**, 66, 363–371; b) M. Ionescu, H. Mantsch, *Adv. Heterocycl. Chem.* **1967**, 8, 83–113; c) C. Bodea, I. Silberg, *Adv. Heterocycl. Chem.* **1968**, 9, 321–460; d) L. Valzelli, S. Garattini in *Principles of Psychopharmacology* (Ed.: W. G. Clark), Academic Press, **1970**, pp. 255–258; e) C. O. Okafor, *Heterocycles* **1977**, 7, 391–427; f) Z. Eckstein, T. Urbanski, *Adv. Heterocycl. Chem.* **1979**, 23, 1–53; g) J. Szabó, *Chem. Heterocycl. Compd.* **1979**, 15, 291–308; h) W. J. Albery, A. W. Foulds, K. J. Hall, A. R. Hillman, R. G. Edgell, A. F. Orchard, *Nature* **1979**, 282, 793–797.
- [16] a) H. Oka, *J. Mater. Chem.* **2008**, 18, 1927–1934; b) T. Okamoto, M. Kuratsu, M. Kozaki, K. Hirotsu, A. Ichimura, T. Matsushita, K. Okada, *Org. Lett.* **2004**, 6, 3493–3496; c) D. Sun, S. V. Rosokha, J. K. Kochi, *J. Am. Chem. Soc.* **2004**, 126, 1388–1401; d) J. K. Kochi, R. Rathore, P. Le Maguères, *J. Org. Chem.* **2000**, 65, 6826–6836; e) T. Nishinaga, R. Inoue, A. Matsuura, K. Komatsu, *Org. Lett.* **2002**, 4, 1435–1438; f) D. Pan, D. L. Phillips, *J. Phys. Chem. A* **1999**, 103, 4737–4743.
- [17] a) R. Duesing, G. Tapolsky, T. J. Meyer, *J. Am. Chem. Soc.* **1990**, 112, 5378–5379; b) W. E. Jones Jr., P. Chen, T. J. Meyer, *J. Am. Chem. Soc.* **1992**, 114, 387–388; c) A. M. Brun, A. Harriman, V. Heitz, J.-P. Sauvage, *J. Am. Chem. Soc.* **1991**, 113, 8657–8663; d) H. D. Burrows, T. J. Kemp, M. J. Welburn, *J. Chem. Soc. Perkin Trans. 2* **1973**, 969–974; e) J.-P. Collin, S. Guillerez, J.-P. Sauvage, *J. Chem. Soc. Chem. Commun.* **1989**, 776–778; f) J. Daub, R. Engl, J. Kurzawa, S. E. Miller, S. Schneider, A. Stockmann, M. R. Wasielewski, *J. Phys. Chem. A* **2001**, 105, 5655–5665.
- [18] a) R. C. Wheland, J. L. Gillson, *J. Am. Chem. Soc.* **1976**, 98, 3916–3925; b) P. Berges, J. Kudnig, G. Klar, E. Sanchez-Martinez, R. Diaz-Calleja, *Synth. Met.* **1992**, 46, 207–219; c) A. Knorr, J. Daub, *Angew. Chem.* **1995**, 107, 2925–2927; *Angew. Chem. Int. Ed. Engl.* **1995**, 34, 2664–2666; d) H. Spreitzer, M. Scholz, G. Gescheidt, J. Daub, *Liebigs Ann.* **1996**, 2069–2077; e) H. Spreitzer, J. Daub, *Chem. Eur. J.* **1996**, 2, 1150–1158.
- [19] a) Ntera Limited, Ire., *Eur. Pat. Appl.*, **2004**, 13 EP 1443090A1 20040804; b) Mitsubishi Electric Corp., Japan, *Jpn. Kokai Tokkyo Koho* **1985**, 4JP 60115681A2 19850622.
- [20] a) X. Kong, A. P. Kulkarni, S. A. Jenekhe, *Macromolecules* **2003**, 36, 8992–8999; b) R. Y. Lai, X. Kong, S. A. Jenekhe, A. J. Bard, *J. Am. Chem. Soc.* **2003**, 125, 12631–12639; c) S. A. Jenekhe, L. Lu, M. M. Alam, *Macromolecules* **2001**, 34, 7315–7324; d) R. Y. Lai, E. F. Fabrizio, L. Lu, S. A. Jenekhe, A. J. Bard, *J. Am. Chem. Soc.* **2001**, 123, 9112–9118; e) A. Higuchi, H. Inada, T. Kobata, Y. Shiraota, *Adv. Mater.* **1991**, 3, 549–550.
- [21] a) L. S. Park, Y. S. Han, D. S. Kim, J. S. Hwang, *Mol. Cryst. Liq. Cryst. Sci. Technol. Sect. A* **2001**, 371, 309–312; b) D.-H. Hwang, S.-K. Kim, M.-J. Park, J.-H. Lee, B.-W. Koo, I.-N. Kang, S.-H. Kim, T. Zyung, *Chem. Mater.* **2004**, 16, 1298–1303.
- [22] Y. S. Han, S. D. Kim, L. S. Park, D. U. Kim, Y. Kwon, *J. Polym. Sci. Part A* **2003**, 41, 2502–2511.

- [23] a) G. R. Hutchison, M. A. Ratner, T. J. Marks, *J. Am. Chem. Soc.* **2005**, *127*, 2339–2350; b) B. Rybtchinski, L. E. Sinks, M. R. Wasielewski, *J. Am. Chem. Soc.* **2006**, *128*, 649–657.
- [24] N. Nambu, S. Sakurai, T. Nagai, *Chem. Pharm. Bull.* **1974**, *22*, 1405–1407.
- [25] B. Xiang, L. Kevan, *Langmuir* **1994**, *10*, 2688–2693.
- [26] a) K. C. Khulbe, R. S. Mann, *J. Catal.* **1988**, *112*, 579–584; b) R. M. Krishna, V. Kurshev, L. Kevan, *Phys. Chem. Chem. Phys.* **1999**, *1*, 2833–2839; c) Z. Luan, J. Y. Bae, L. Kevan, *Chem. Mater.* **2000**, *12*, 3202–3207; d) Z. Luan, L. Kevan, *Stud. Surf. Sci. Catal.* **2001**, *135*, 3871–3877; e) Z. Luan, J. Y. Bae, L. Kevan, *Microporous Mesoporous Mater.* **2001**, *48*, 189–194.
- [27] a) A. W. Franz, Z. Zhou, R. Turdean, A. Wagener, B. Sarkar, M. Hartmann, S. Ernst, W. R. Thiel, T. J. J. Müller, *Eur. J. Org. Chem.* **2009**, 3895–3905; b) Z. Zhou, A. W. Franz, M. Hartmann, A. Seifert, T. J. J. Müller, W. R. Thiel, *Chem. Mater.* **2008**, *20*, 4986–4992.
- [28] E. F. Godefroi, E. L. Wittle, *J. Org. Chem.* **1956**, *21*, 1163–1168.
- [29] T. Schareina, A. Zapf, M. Beller, *Chem. Commun.* **2004**, 1388–1389.
- [30] A. W. Franz, L. N. Popa, T. J. J. Müller, *Tetrahedron Lett.* **2008**, *49*, 3300–3303.
- [31] S. van der Laan, B. L. Feringa, R. M. Kellogg, J. van Esch, *Langmuir* **2002**, *18*, 7136–7140.
- [32] J. J. E. Moreau, B. P. Pichon, C. Bied, M. W. C. Man, *J. Mater. Chem.* **2005**, *15*, 3929–3936.
- [33] F. P. Schmidtchen, M. Berger, *Chem. Rev.* **1997**, *97*, 1609–1646.
- [34] E. J. Cho, J. W. Moon, S. W. Ko, J. Y. Lee, S. K. Kim, J. Yoon, K. C. Nam, *J. Am. Chem. Soc.* **2003**, *125*, 12376–12377.
- [35] a) N. Hovnanian, S. Cerneaux, P. Dieudonne, *J. Sol-Gel Sci. Technol.* **2004**, *31*, 353–358; b) Y. Luo, P. Yang, J. Lin, *Microporous Mesoporous Mater.* **2008**, *111*, 194–199; c) M. Álvaro, M. Benitez, D. Das, B. Ferrer, H. García, *Chem. Mater.* **2004**, *16*, 2222–2228; d) M. Benitez, D. Das, R. Ferreira, U. Pischel, H. García, *Chem. Mater.* **2006**, *18*, 5597–5603.
- [36] L. Yang, J.-K. Feng, A.-M. Ren, *J. Org. Chem.* **2005**, *70*, 5987–5996.
- [37] M. Jia, A. Seifert, M. Berger, H. Giegengack, S. Schulze, W. R. Thiel, *Chem. Mater.* **2004**, *16*, 877–882.
- [38] K. Moller, T. Bein, R. X. Fischer, *Chem. Mater.* **1999**, *11*, 665–673.
- [39] M. T. Anderson, J. E. Martin, J. G. Odinek, P. P. Newcomer, *Chem. Mater.* **1998**, *10*, 1490–1500.
- [40] Q. Huo, D. I. Margolese, G. D. Stucky, *Chem. Mater.* **1996**, *8*, 1147–1160.
- [41] B. Marler, U. Oberhagemann, S. Vortmann, H. Gies, *Microporous Mater.* **1996**, *6*, 375–383.
- [42] M. Kruk, M. Jaroniec, A. Sayari, *J. Phys. Chem. B* **1999**, *103*, 4590–4598.
- [43] M. H. Lim, C. F. Blanford, A. Stein, *J. Am. Chem. Soc.* **1997**, *119*, 4090–4091.
- [44] J. C. Vartuli, K. D. Schmitt, C. T. Kresge, W. J. Roth, M. E. Leonowicz, S. B. McCullen, S. D. Hellring, J. S. Beck, J. L. Schlenker, *Chem. Mater.* **1994**, *6*, 2317–2326.
- [45] Q. Huo, D. I. Margolese, U. Ciesla, D. G. Demuth, P. Feng, T. E. Gier, P. Sieger, A. Firouzi, B. F. Chmelka, *Chem. Mater.* **1994**, *6*, 1176–1191.
- [46] R. Huq, L. Mercier, P. J. Kooyman, *Chem. Mater.* **2001**, *13*, 4512–4519.
- [47] M. C. Holmes, *Curr. Opin. Colloid Interface Sci.* **1998**, *3*, 485–492.
- [48] U. Henriksson, E. S. Blackmore, G. J. T. Tiddy, O. Soederman, *J. Phys. Chem.* **1992**, *96*, 3894–3902.
- [49] Z. Zhang, Y. Han, F.-S. Xiao, S. Qiu, L. Zhu, R. Wang, Y. Yu, Z. Zhang, B. Zou, Y. Wang, H. Sun, D. Zhao, Y. Wei, *J. Am. Chem. Soc.* **2001**, *123*, 5014–5021.
- [50] R. K. Iler, *The Chemistry of Silica*, Wiley, New York, **1971**.
- [51] X. Liu, B. Tian, C. Yu, F. Gao, S. Xie, B. Tu, R. Che, L.-M. Peng, D. Zhao, *Angew. Chem.* **2002**, *114*, 4032–4034; *Angew. Chem. Int. Ed.* **2002**, *41*, 3876–3878.
- [52] A. Monnier, F. Schüth, Q. Huo, D. Kumar, D. Margolese, R. S. Maxwell, G. D. Stucky, M. Krishnamurty, P. Petroff, A. Firouzi, M. Janicke, B. F. Chmelka, *Science* **1993**, *261*, 1299–1303.
- [53] E. P. Barrett, L. G. Joyner, P. P. Halenda, *J. Am. Chem. Soc.* **1951**, *73*, 373–380.
- [54] K. S. W. Sing, D. H. Everett, R. A. W. Haul, L. Moscou, R. A. Pierotti, J. Rouquerol, T. Siemieniewska, *Pure Appl. Chem.* **1985**, *57*, 603–619.
- [55] P. I. Ravikovitch, S. C. Odomhnaill, A. V. Neimark, F. Schüth, K. K. Unger, *Langmuir* **1995**, *11*, 4765–4772.
- [56] F. Rojas, I. Kornhauser, C. Felipe, J. M. Esparza, S. Cordero, A. Dominguez, J. L. Riccardo, *Phys. Chem. Chem. Phys.* **2002**, *4*, 2346–2355.
- [57] A. Corma, Q. B. Kan, M. T. Navarro, J. Perez-Pariente, F. Rey, *Chem. Mater.* **1997**, *9*, 2123–2126.
- [58] A. V. Neimark, P. I. Ravikovitch, M. Grun, F. Schüth, K. K. Unger, *J. Colloid Interface Sci.* **1998**, *207*, 159–169.
- [59] a) M. H. Lim, C. F. Blanford, A. Stein, *Chem. Mater.* **1998**, *10*, 467–470; b) S. L. Burkett, S. D. Sims, S. Mann, *Chem. Commun.* **1996**, 1367–1368; c) C. E. Fowler, S. L. Burkett, S. Mann, *Chem. Commun.* **1997**, 1769–1770.
- [60] C. E. Fowler, S. Mann, B. Lebeau, *Chem. Commun.* **1998**, 1825–1826.
- [61] A. Corma, *Chem. Rev.* **1997**, *97*, 2373–2419.
- [62] R. Richer, L. Mercier, *Chem. Mater.* **2001**, *13*, 2999–3008.
- [63] S. M. Gruner, *J. Phys. Chem.* **1989**, *93*, 7562–7570.
- [64] C. J. Brinker, G. W. Scherer, *Sol-Gel Science*, Academic Press, Boston, **1990**.
- [65] J. M. Thomas, O. Terasaki, P. L. Gai, W. Z. Zhou, J. Gonzalez-Calbet, *Acc. Chem. Res.* **2001**, *34*, 583–594.
- [66] S. Huh, J. W. Wiench, J. C. Yoo, M. Pruski, V. S. Y. Lin, *Chem. Mater.* **2003**, *15*, 4247–4256.
- [67] S. Huh, J. W. Wiench, B. G. Trewyn, S. Song, M. Pruski, V. S. Y. Lin, *Chem. Commun.* **2003**, 2364–2365.
- [68] N. B. Colthup in *An Introduction to Infrared and Raman Spectroscopy* (Eds.: L. H. Daly, S. E. Wiberley), Academic Press, Boston, **1990**.
- [69] L. P. Kuhn, *J. Am. Chem. Soc.* **1952**, *74*, 2492–2499.
- [70] J. Jadzyn, M. Stockhausen, B. Zywicki, *J. Phys. Chem.* **1987**, *91*, 754–757.
- [71] X. S. Zhao, G. Q. Lu, A. K. Whittaker, G. J. Millar, H. Y. Zhu, *J. Phys. Chem. B* **1997**, *101*, 6525–6531.
- [72] M. Fröba, P. Behrens, J. Wong, G. Engelhardt, C. Haggemüller, G. Vandegoor, M. Rowen, T. Tanaka, W. Schwieger in *Advances in Porous Materials*, (Eds.: S. Komarneni, D. M. Smith, J. S. Beck), Materials Research Soc., Pittsburgh, **1995**, pp. 99–104.
- [73] D. W. Sindorf, G. E. Maciel, *J. Am. Chem. Soc.* **1981**, *103*, 4263–4265.
- [74] S. M. De Paul, J. W. Zwanziger, R. Ulrich, U. Wiesner, H. W. Spiess, *J. Am. Chem. Soc.* **1999**, *121*, 5727–5736.
- [75] S. Ek, E. I. Iiskola, L. Niinistö, J. Vahtinen, T. T. Pakkanen, A. Root, *J. Phys. Chem. A* **2004**, *108*, 11454–11463.
- [76] D. Fattakhova Rohlfling, J. Rathousky, Y. Rohlfling, O. Bartels, M. Wark, *Langmuir* **2005**, *21*, 11320–11329.
- [77] A. J. Bard, L. R. Faulkner, *Electrochemical Methods Fundamentals and Applications*, Wiley, New York, **2001**.
- [78] R. W. Murray, *Chemically Modified Electrodes in Electroanalytical Chemistry, A Series of Advances, Vol. 13*, New York, **1984**.
- [79] Y. Guo, A. Mylonakis, Z. Zhang, G. Yang, P. I. Lelkes, S. Che, Q. Lu, Y. Wei, *Chem. Eur. J.* **2008**, *14*, 2909–2917.
- [80] A. Doménech, M. Alvaro, B. Ferrer, H. Garcia, *J. Phys. Chem. B* **2003**, *107*, 12781–12788.
- [81] N. C. Maiti, S. Mazumdar, N. Periasamy, *J. Phys. Chem. B* **1998**, *102*, 1528–1538.
- [82] G. R. Hutchison, M. A. Ratner, T. J. Marks, *J. Am. Chem. Soc.* **2005**, *127*, 16866–16881.
- [83] P. A. Leermakers, H. T. Thomas, L. D. Weis, F. C. James, *J. Am. Chem. Soc.* **1966**, *88*, 5075–5083.
- [84] E. H. A. Beckers, S. C. J. Meskers, A. P. H. J. Schenning, Z. Chen, F. Würthner, P. Marsal, D. Beljonne, J. Cornil, R. A. J. Janssen, *J. Am. Chem. Soc.* **2006**, *128*, 649–657.
- [85] M. Sailer, A. W. Franz, T. J. J. Müller, *Chem. Eur. J.* **2008**, *14*, 2602–2614.

- [86] a) P. L. Maguères, S. V. Lindeman, J. K. Kochi, *J. Chem. Soc. Perkin Trans. 2* **2001**, 1180–1185; b) B. Badger, B. Brocklehurst, *Nature* **1968**, 219, 263–263.
- [87] A. Ortiz, I. Poyato, J. I. Fernandez-Alonso, *J. Pharm. Sci.* **1983**, 72, 50–55.
- [88] *Organikum*, 21st ed. (Eds.: H. G. O. Becker, R. Beckert, G. Domschke, E. Fanghänel, W. D. Habicher, P. Metz, D. Pavel, K. Schwetlick), Wiley-VCH, Weinheim, **2001**.
- [89] M. Hesse, H. Meier, B. Zeeh, *Spektroskopische Methoden in der Organischen Chemie*, Georg Thieme Verlag, Stuttgart, **1991**, pp. 69.
- [90] P. Zanello in *Ferrocenes* (Eds.: A. Togni, T. Hayashi), VCH, Weinheim, **1995**, pp. 317.

Received: March 31, 2010
Published online: August 2, 2010